SCIENTIFIC REP⚙RTS

Magnetically-induced ferroelectricity in the $(ND_4)_2[FeCl_5(D_2O)]$ molecular compound

José Alberto Rodríguez-Velamazán[1,2], Óscar Fabelo[2], Ángel Millán[1], Javier Campo[1], Roger D. Johnson[3] & Laurent Chapon[2]

The number of magnetoelectric multiferroic materials reported to date is scarce, as magnetic structures that break inversion symmetry and induce an improper ferroelectric polarization typically arise through subtle competition between different magnetic interactions. The $(NH_4)_2[FeCl_5(H_2O)]$ compound is a rare case where such improper ferroelectricity has been observed in a molecular material. We have used single crystal and powder neutron diffraction to obtain detailed solutions for the crystal and magnetic structures of $(NH_4)_2[FeCl_5(H_2O)]$, from which we determined the mechanism of multiferroicity. From the crystal structure analysis, we observed an order-disorder phase transition related to the ordering of the ammonium counterion. We have determined the magnetic structure below T_N, at 2 K and zero magnetic field, which corresponds to a cycloidal spin arrangement with magnetic moments contained in the ac-plane, propagating parallel to the c-axis. The observed ferroelectricity can be explained, from the obtained magnetic structure, via the inverse Dzyaloshinskii-Moriya mechanism.

Multiferroic materials, compounds presenting at least two ferroic- orders simultaneously, have attracted considerable interest due to the possible cross control of physical properties. In particular, magnetoelectric multiferroics where an electrical polarization is induced by a magnetic transition, the so-called type-II multiferroics, have been extensively studied for their fundamental properties as well as for their potential applications in memories, sensors, transducers, etc.[1].

The complex magnetic ordered state in these improper (or pseudo-proper) ferroelectric materials[2] is stabilized by competitions between different exchange couplings which break inversion symmetry and induce a ferroelectric polarization. The most studied multiferroics of this type are the "cycloidal" magnets such as $RMnO_3$[3–6] $MnWO_4$[7–9] or $CoCr_2O_4$[10,11], where ferroelectricity emerges as a consequence of a cycloidal modulation of the magnetic moments. The coupling mechanism between magnetization and ferroelectricity has been explained by the so-called *inverse* Dzyaloshinskii-Moriya (DM) effect[12,13] or spin current mechanism, that predict that the electric polarization, **P**, is proportional to $\mathbf{r}_{ij} \times (\mathbf{S}_i \times \mathbf{S}_j)$, where $\mathbf{r}_{ij}$ is the vector connecting the nearest spins, $\mathbf{S}_i$ and $\mathbf{S}_j$, and $(\mathbf{S}_i \times \mathbf{S}_j)$ is the so-called spin-chirality vector[14].

One of the approaches to the design of materials combining different properties is the association of different building blocks that carry the different properties of interest. When a ferroelectric material is wanted, the use of ammonium molecules substituting monovalent counterions (i.e. Na, K, Rb or Cs) in inorganic networks has been proved as a successful approach in order to induce a switchable ferroelectric transition. This is the case of peroxychromates of general formula M_3CrO_8[15,16], where the substitution of

[1]Instituto de Ciencia de Materiales de Aragón (ICMA), CSIC – Universidad de Zaragoza, 50009 Zaragoza, Spain. [2]Institut Laue-Langevin, 38042 Grenoble Cedex 9, France. [3]Univ. Oxford, Dept Phys, Clarendon Lab, Oxford OX1 3PU, England. Correspondence and requests for materials should be addressed to O.F. (email: fabelo@ill.eu) or L.C. (email: chapon@ill.fr)

the alkali metals by an ammonium molecule produces a system with a well-defined ferroelectric phase transition[17,18]. A similar approach has been used in metal-organic compounds, where the combination of two different networks with different properties has been shown to be an excellent strategy to design new multiferroic materials[19–24]. Nevertheless, in all these examples the existence of ferroelectric or antiferro-electric transitions is due to the occurrence of an order−disorder phase transition where the hydrogen bonds between the guest molecule and the host-framework play a central role. No interplay between the magnetic and electric orders has been observed in these cases, and therefore improper ferroelectricity has never been described for this type of compounds. However, a recently published work focused on ammonium pentacloroaquaferrate(III), with formula $(NH_4)_2[FeCl_5(H_2O)]$, has characterized this molec-ular compound as a new multiferroic material, where magnetic and electric properties are connected[25]. The heat capacity of the deuterated sample, of formula $(ND_4)_2[FeCl_5(D_2O)]$ (see Supplementary Figure S1), shows a behavior equivalent to that of the hydrogenated sample reported by Ackermann *et al.*[25], pre-senting two closely spaced peaks in the low temperature region at ca. 6.9 and 7.2 K[25,26]. At high tempera-ture (*ca* 79 K), this material reveals a third signal in the heat capacity, associated to a suspected structural phase transition, although the previous X-ray diffraction measurements above and below this transition did not show any significant changes[25]. The single crystal susceptibility measurements indicate an *XY* ani-sotropy with the *ac*-plane being the magnetic easy plane. The spontaneous electric polarization obtained integrating the pyroelectric current shows that the system becomes ferroelectric below $T_{FE} \sim 6.9$ K at zero magnetic field, corresponding with the low temperature cusp in the heat capacity. The polarization has two components: the main one along the *a*-axis with a value of $3 \mu Cm^{-2}$ and a secondary one, with a value ten times lower, along the *b*-axis. Thus, the spontaneous electric polarization lies in the *ab*-plane.

In this paper, we investigate the temperature dependence of the crystal structure using X-ray and neutron diffraction measurements (on hydrogenated and deuterated samples respectively). Below T_N, (at 2 K) we have determined unambiguously the magnetic structure at zero magnetic field. A simple model based on a set of four exchange coupling interactions has been proposed to explain the magnetic ground state. We present also the temperature evolution of some selected magnetic reflections in order to evaluate the possible spin-reorientation above 6.9 K. Finally, we propose the possible multiferroicity mechanism in the $(ND_4)_2[FeCl_5(D_2O)]$ compound.

Results

Neutron Studies. *Crystal structure at 100 K.* The title compound is built up from one $[FeCl_5(D_2O)]^{2-}$ ion and two ND_4 counterions, and the crystal structure is held together by an extensive network of H-bonds in concurrence with the ionic interaction (see Fig. 1). The Kitaigorodskii Packing Index (KPI) gives a percent of filled space of 81.5[27], therefore there is no accessible space in the network for solvents. The crystallographic properties of the two phases (above and below the structural phase transition), including space groups, lattice parameters as well as some details of the data refinement, are shown in Table 1.

The Fe(III) atom is located on a mirror plane perpendicular to the *b*-axis, and presents a slightly distorted octahedral environment. The shortest Fe-Cl bond distances correspond to Cl(1), which is coor-dinated in *trans-* conformation with respect to the water molecule (see Table 2). The interbond angles in the anion are slightly different of those of an ideal octahedron. These deviations are related with the strength of the different hydrogen bonds present in this compound. A clear example is the coordination water molecule hydrogen bond [O(1w)-D⋯Cl(2)], with a D⋯Cl distance of 2.217(2) Å. As result of this interaction the Fe-Cl(2) bond distances are slightly elongated. The influence of the H-bonds due to the ND_4 counterion is more difficult to quantify due to the extension of the H-bond network in which the ND_4 molecule is involved. A detailed list with all the possible H-bonds can be consulted in Table 3.

The refinement of the ND_4 molecule at high temperature was made by several successive attempts. Our first model considered the ND_4 molecule ordered. An initial model was obtained using soft con-straints, with the ND_4 molecule geometrically fixed and only small deviations of this ideal geometry allowed. A similar protocol was also applied using rigid bodies as implemented in FullProf suite[28,29] but in that case the ND_4 molecule forms an undeformable rigid body with a perfect tetrahedral symmetry. In order to define a realistic model, the N-D bond length was fixed at 1.025 Å and the D-N-D angle was fixed to 109°, values in agreement with other ammonium-containing compounds[30,31]. The values of the Fe–Cl, Fe-O and O-D bond lengths were left variable. Unfortunately all our attempts to refine this model produce unstable solutions. A more complex model considering the ND_4 molecule disordered was subsequently tested. For the starting point of this model, the D atoms of the ND_4 molecule were set in 8 different sites (Wyckoff position 8*d*) with an occupancy of 0.5 that is equivalent to two disordered ND_4 units with half occupancy. The first set of refinements was made using the Simulated Annealing proce-dure included on the FullProf suite[28,29]. The refinement produced a solution where the 8 D atoms around the N can be seen as two superimposed tetrahedrons (see Fig. 1). This model was the starting point for the latter refinement using the SHELX program[32]. The final refinement was made without restraints. The values of the N-D bond distances as well as the D-N-D angles are in agreement with those observed in other ammonium-containing compounds[30,31].

The deuterium atoms of the disordered ND_4 act as donors in an extensive hydrogen-bond network where each deuterium is involved in a single H-bond, with distances ranging from 2.329(4) to 2.540(6) Å.
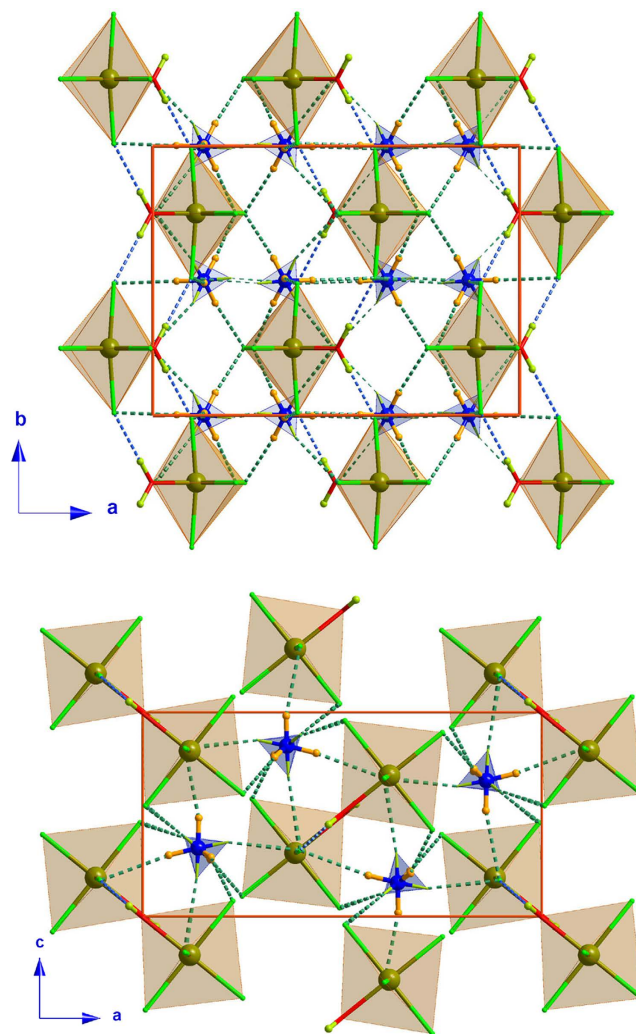
Figure 1. Views of the 100 K crystal packing along the *c*-axis (top) and *b*-axis (bottom) of the $(ND_4)_2[FeCl_5(D_2O)]$ compound, where the O-D⋯Cl and the N-D⋯Cl hydrogen bonds have been represented as blue and green dashed lines, respectively. For the sake of clarity only one conformation of the disordered ND_4 molecule has been drawn in polyhedron representation.

The shortest H-bonds are those involving the coordinated water molecule and both *trans*-Cl(2) atoms, which connect the Iron(III) atoms forming a zig-zag chain along the *b*-axis.

The shortest Fe⋯Fe distance connects iron atoms in the Fe(1)-O(1w)-D⋯Cl(2)-Fe(1) zig-zag chain running along the *b*-axis, with a distance between metallic centers of 6.457(1) Å, while the shortest interchain distance connects the Fe atoms within the *ac*-plane, with a distance of 6.8125(14) Å.

Crystal structure determination at low temperature. There have been several previous attempts to refine the crystal structure of this compound at low temperature (below the structural phase transition)[25,33]; nevertheless, the reported structures above and below the phase transition were mainly the same, and neither changes in the space group nor a significant displacement on the atomic positions were observed. These observations have been also verified in this work with X-ray single crystal diffraction data collections above and below the nuclear phase transition. The best model fitting the X-ray data is always obtained with the structure refined on the space group *Pnma*, independently of the temperature (in our case RT and 45 K, see Supplementary Information for details). These results suggest that the hydrogen atoms present in the structure are responsible for the phase transition, and therefore neutron diffraction would be a well suited probe to analyze it due to the good contrast provided for light atoms. In order to verify our hypothesis, neutron diffraction measurements of the deuterated compound have been carried out on a powder sample (at 45 K) and on a single crystal (at 100 and 2 K).

Assuming that the possible phase transition is a second order ("continuous") phase transition, we determined the list of possible subgroups of the high temperature space group (*Pnma*). The only possible space groups are ***Pna2_1*** (No. 33), ***Pmn2_1*** (No. 31), ***Pmc2_1*** (No. 26), $P2_12_12_1$ (No. 19), $P2_1/c$ (No. 14), $P2_1/m$ (No. 11), ***Pc*** (No. 7), ***Pm*** (No. 6), ***P2_1*** (No. 4), *P*-1 (No. 2) and ***P1*** (No. 1), where the polar

Formula	[ND$_4$]$_2$[Fe^{III}Cl$_5$(D$_2$O)]	
Empirical Formula	Cl$_5$D$_{10}$FeN$_2$	
M$_r$ (g·mol^{-1})	297.26	
Temperature (K)	100(2)	2(2)
Inst. λ(Å)	D9, 0.83220	D9, 0.83220
Crystal system	Orthorhombic	Monoclinic
Space group (No.)	*Pnma* (62)	*P*112$_1$/*a* (14)
Crystal size (mm)	3 × 3 × 3	3 × 3 × 3
a (Å)	13.5221(9)	13.5019(7)
b (Å)	9.9305(6)	9.9578(5)
c (Å)	6.9219(6)	6.9049(4)
α(°)	90.00	90.00
β(°)	90.00	90.00
γ(°)	90.00	90.109(4)
V (Å^3)	929.48(12)	928.36(9)
Z	4	4
ρ$_c$ (g·cm^{-3})	2.124	2.127
Meas. Reflections/(R$_{int}$)	2710 (0.0270)	4900 (0.0234)
Indep. ref. [I > 2σ(I)]	1328	1673
Parameters/restraints.	132/ 0	174/0
Hydrogen treatment	Refall	Refall
Goodness of fit	1.111	0.976
Final R indices [I > 2σ(I)]: R$_1$/wR$_2$	0.0431/0.0980	0.0402/0.0966
R indices (all data): R$_1$/wR$_2$	0.0484/0.1010	0.0605/0.0988

Table 1. Experimental parameters and main structural crystallographic data for the studied compounds. The crystallographic details of the data collections at RT and 50 K using single crystal X-ray diffraction have been provided in the Supplementary Information (see text and Supplementary Table S1).

ones are written in bold. Given that the structural transition (ca 79 K) is not associated with the onset of a ferroelectric state[25], the only possible space groups immediately below this phase transition are in principle the non-polar ones. Once the system becomes ferroelectric below 6.9 K, these non-polar groups are no more strictly correct, but the structural changes responsible of this type of electric polarization are usually too subtle to be observable[4], so we assumed the same space group at 45 K and 2 K. All possible space groups were tested by trial and error and the only subgroup that refines properly the experimental data was found to be *P*2$_1$/*c* (No. 14). However, in order to facilitate comparisons between the high- (100 K) and low-temperature phases the refinement was carried out in the *P*112$_1$/*a* space group, which is a non-standard setting of *P*2$_1$/*c* (No. 14). The reflection splitting due to the subtle monoclinic distortion can be clearly observed in the high resolution neutron powder diffraction data at 45 K (see Supplementary Figure S2).

The results of the refinement of the single crystal data show a crystal structure at low temperature which is built up from one and two crystallographically independent [FeCl5·H2O]$^{2-}$ and ND$_4$ units, respectively (see Fig. 2). As previously mentioned, the low temperature phase crystalizes in *P*112$_1$/*a* space group, which is a maximal non-isomorphic subgroup of *Pnma* with index 2. Therefore the number of crystallographically independent atoms at low temperature is doubled with respect to the high temperature phase. The phase transition involves the loss of a *n*-glide parallel to the *a*-axis and a mirror plane which is contained in the *ac*-plane, together with a slight variation in the cell parameters and the cell volume (see Table 1). The KPI packing index gives a percent of filled space of 77.2, a value which is slightly lower than that observed at high temperature[27]. However, as it occurs in the high-temperature phase, there is no accessible space in the network for solvents.

At low temperature, the Fe(III) atoms are located on a *4e* general position due to the loss of the mirror plane perpendicular to the *b*-axis. The Fe(III) environment is slightly more distorted compared with the high temperature structure, but the octahedral environment is held. The largest variations are observed in the long bond distances involving Cl(1), Cl(2) and Cl(5), where a significant elongation of the Fe-Cl distance has been identified (see Table 2). The interbond angles in the anion are very similar to those observed at high temperature (see Table 2).

100K		2 K	
Distances (Å)		Distances (Å)	
Fe(1)-O(1W)	2.095(2)	Fe(1)-O(1w)	2.095(2)
Fe(1)-Cl(1)	2.3155(15)	Fe(1)-Cl(1)	2.391(2)
Fe(1)-Cl(2)	2.3926(7)	Fe(1)-Cl(2)	2.400(2)
Fe(1)-Cl(2)[a]	2.3926(7)	Fe(1)-Cl(3)	2.3375(14)
Fe(1)-Cl(3)	2.3435(16)	Fe(1)-Cl(4)	2.3179(13)
Fe(1)-Cl(4)	2.3892(16)	Fe(1)-Cl(5)	2.4026(14)
N(1)-D(1A)	1.035(6)	N(1)-D(1)	1.027(3)
N(1)-D(2A)	0.959(5)	N(1)-D(2)	1.007(4)
N(1)-D(3A)	1.013(5)	N(1)-D(3)	1.004(2)
N(1)-D(4A)	1.015(5)	N(1)-D(4)	1.026(3)
N(1)-D(1B)	1.026(3)	N(2)-D(5)	1.012(3)
N(1)-D(2B)	1.019(5)	N(2)-D(6)	1.027(4)
N(1)-D(3B)	1.008(4)	N(2)-D(7)	1.026(3)
N(1)-D(4B)	0.970(4)	N(2)-D(8)	1.018(3)
O(1w)-D(1w)	0.958(2)	O(1W)-D(1W)	0.963(4)
		O(1W)-D(2W)	0.973(4)
Angles (°)		Angles (°)	
Cl(1)-Fe(1)-Cl(2)	94.40(1)	Cl(1)-Fe(1)-Cl(2)	170.73(1)
Cl(1)-Fe(1)-Cl(2)[a]	94.40(1)	Cl(1)-Fe(1)-Cl(3)	90.53(1)
Cl(1)-Fe(1)-Cl(3)	90.49(1)	Cl(1)-Fe(1)-Cl(4)	94.78(1)
Cl(1)-Fe(1)-Cl(4)	89.86(1)	Cl(1)-Fe(1)-Cl(5)	89.61(1)
Cl(1)-Fe(1)-O(1W)	179.76(1)	Cl(1)-Fe(1)-O(1W)	85.51(1)
Cl(2)-Fe(1)-Cl(2)[a]	171.08(1)	Cl(2)-Fe(1)-Cl(3)	91.23(1)
Cl(2)-Fe(1)-Cl(3)	90.70(1)	Cl(2)-Fe(1)-Cl(4)	94.29(1)
Cl(2)-Fe(1)-Cl(4)	89.28(1)	Cl(2)-Fe(1)-Cl(5)	88.55(1)
Cl(2)-Fe(1)-O(1W)	85.60(1)	Cl(2)-Fe(1)-O(1W)	85.40(1)
Cl(3)-Fe(1)-Cl(2)[a]	90.70(1)	Cl(3)-Fe(1)-Cl(4)	90.74(1)
Cl(3)-Fe(1)-Cl(4)	179.64(1)	Cl(3)-Fe(1)-Cl(5)	179.44(1)
Cl(3)-Fe(1)-O(1W)	89.75(1)	Cl(3)-Fe(1)-O(1W)	89.87(1)
Cl(4)-Fe(1)-Cl(2)[a]	89.28(1)	Cl(4)-Fe(1)-Cl(5)	89.78(1)
Cl(4)-Fe(1)-O(1W)	89.90(1)	Cl(4)-Fe(1)-O(1W)	179.32(1)
O(1W)-Fe(1)-Cl(2)[a]	85.60(1)	Cl(5)-Fe(1)-O(1W)	89.60(1)
D(1W)-O(1W)-D(1W)[a]	110(1)	D(1W)-O(1W)-D(2W)	109(1)

Table 2. Main structural variations between high and low temperature phases obtained from single crystal neutron diffraction refinement. [a]Symmetry codes: x, $0.5-y$, z.

The most remarkable difference between high- and low-temperature phases concerns the ND_4 counterions which are well ordered below the phase transition (ca 79 K). An order-disorder transition is therefore proposed as the origin of this structural phase transition. The influence of the H-bond network in this transition has been taken into account by analyzing the bond-distances and the bond-orientation. At low-temperature all the bond-distances are slightly shorter than those observed at high-temperature. The bond-orientations are very similar, and in both cases the donor atoms interact with only one acceptor, so the structural transition can be seen as the splitting of the previously disordered ammonium into two independent positions, triggered by an reduction of the ND···Cl bond distances between the ND_4 molecules and the $[FeCl5·H2O]^{2-}$ units (see Fig. 3). A detailed list with all the possible H-bonds can be consulted in Table 3.

The Fe···Fe distance along the zig-zag chain running along the b-axis is slightly longer than the observed at high temperature, with a value of 6.466(2) Å, while the interchain distance, which connects the Fe atoms in the ac-plane, is Fe···Fe 6.8061(13) Å, slightly longer compared with the high temperature one.

D-H⋯A*	H⋯A/Å	D-H⋯A/°
100 K		
O(1W)-D(1W)⋯Cl(2)[b]	2.217(2)	178.39(14)
N(1)-D(1A)⋯Cl(2)[c]	2.540(6)	173.5(4)
N(1)-D(2A)⋯Cl(4)[d]	2.364(6)	160.8(4)
N(1)-D(3A)⋯Cl(4)	2.368(5)	171.3(4)
N(1)-D(4A)⋯Cl(2)[e]	2.484(6)	160.1(4)
N(1)-D(1B)⋯Cl(2)[d]	2.466(3)	173.6(2)
N(1)-D(2B)⋯Cl(2)[a]	2.418(5)	164.7(4)
N(1)-D(3B)⋯Cl(1)[f]	2.329(4)	169.7(3)
N(1)-D(4B)⋯Cl(3)[g]	2.355(4)	159.6(3)
2 K		
O(1w)-D(1w)⋯Cl(2)[h]	2.217(4)	175.8(3)
O(1w)-D(2w)⋯Cl(1)[i]	2.211(4)	178.3(3)
N(1)-D(1)⋯Cl(5)	2.314(3)	173.3(2)
N(1)-D(2)⋯Cl(5)[j]	2.334(4)	159.4(3)
N(1)-D(3)⋯Cl(1)[g]	2.454(2)	178.3(2)
N(1)-D(4)⋯Cl(1)[f]	2.399(3)	161.4(2)
N(2)-D(5)⋯Cl(2)[h]	2.391(2)	175.8(2)
N(2)-D(6)⋯Cl(3)	2.286(4)	162.0(3)
N(2)-D(7)⋯Cl(2)[k]	2.374(3)	163.8(2)
N(2)-D(8)⋯Cl(4)[l]	2.312(3)	169.2(3)

Table 3. Relevant hydrogen bonds for 100 K and 2 K measurements obtained from single crystal neutron diffraction refinement. *D and A stand for donor and acceptor, respectively. [a]Symmetry codes: x, $0.5 - y$, z. [b]$2 - x$, $-0.5 + y$, $-z$. [c]x, $0.5 - y$, $1 + z$. [d]$2 - x$, $-0.5 + y$, $1 - z$. [e]$1.5 - x$, $-0.5 + y$, $0.5 + z$. [f]$1.5 - x$, $-y$, $0.5 + z$. [g]x, y, $1 + z$. [h]$2 - x$, $1 - y$, $-z$. [i]$2 - x$, $-y$, $-z$. [j]$2 - x$, $-y$, $1 - z$. [k]x, y, $-1 + z$. [l]$1.5 - x$, $1 - y$, $-0.5 + z$.

....

Magnetic Structure. The magnetic structure of $(ND_4)_2[FeCl_5(D_2O)]$ was obtained from single-crystal neutron diffraction data taken at 2 K. is. A survey of reciprocal space was carried out with a series of Q-scans in the first Brillouin zone showing the appearance of superlattice reflections indexed by a prop-agation vector parallel to the c-axis, $\mathbf{k} = (0, 0, k_z)$, with $k_z = 0.2288(4)$. This corresponds to a period of 30.2 Å in real space. In the following section, the magnetic structure is described by labeling the four Fe(III) atoms in the primitive unit-cell as Fe(1), Fe(2), Fe(3) and Fe(4) respectively with crystallographic coordinates (0.388, 0.249, 0.313), (0.119, 0.751, 0.813), (0.619, 0.751, 0.687) and (0.881, 0.249, 0.187). The magnetic moment [$\mathbf{m}_l(j)$] for atoms at positions Fe(j) ($j = 1$ to 4) in the unit-cell l, can be calculated by means of the Fourier expansion:

$$\mathbf{m}_l(j) = \mathbf{Re}(Sj)\cos\{2\pi \cdot [\mathbf{k} \cdot \mathbf{R}_l + \varphi(j)]\} + \mathbf{Im}(Sj)\sin\{2\pi \cdot [\mathbf{k} \cdot \mathbf{R}_l + \varphi(j)]\} \qquad (1)$$

where $\mathbf{R}_l$, is the position vector of the unit-cell l with respect to the origin $\mathbf{R}_l = l_1\mathbf{a} + l_2\mathbf{b} + l_3\mathbf{c}$, where l_i are integers, $\varphi(j)$ are relative phases (in fractions of 2π) and $\mathbf{Re}(Sj)$ and $\mathbf{Im}(Sj)$ are the real and imaginary parts of the Fourier vectors for each site j.

In order to determine the possible magnetic structures compatible with the crystallographic space group ($P112_1/a$) and with the $\mathbf{k} = (0, 0, k_z)$ propagation vector, we have used representational analysis as described initially by Bertaut[34]. The decomposition of the magnetic representation (Γ) in the group of the wave-vector (little group) involves two one-dimensional irreducible representations (Γ_1 and Γ_2). In this symmetry group, only Fe(1)/Fe(2) on one hand, and Fe(3)/Fe(4) on the other, are related by symmetry elements, so that the orbit splits into two sets. For each of them, $\Gamma = 3\Gamma_1 + 3\Gamma_2$, generating three sets of basis vectors for each representation (Table 4).

Magnetic structures compatible with a single representation (magnetic space group $P112/a1'(0,0,g)00s$) have been tested for all combinations of the real and imaginary parts of the Fourier vectors S(j) (i.e. describing all collinear and non-collinear magnetic arrangements). In all cases, the refinements lead to poor agreement factors (over 25% R_F^2) and therefore these solutions can be excluded. In particular, the amplitude-modulated models systematically overestimate the Fe(III) magnetic moment, with amplitude maxima of 5.23(3) μ_B, not physically meaningful. It deserves to be noted that none of these magnetic models would generate a macroscopic ferroelectric polarization, as observed experimentally.
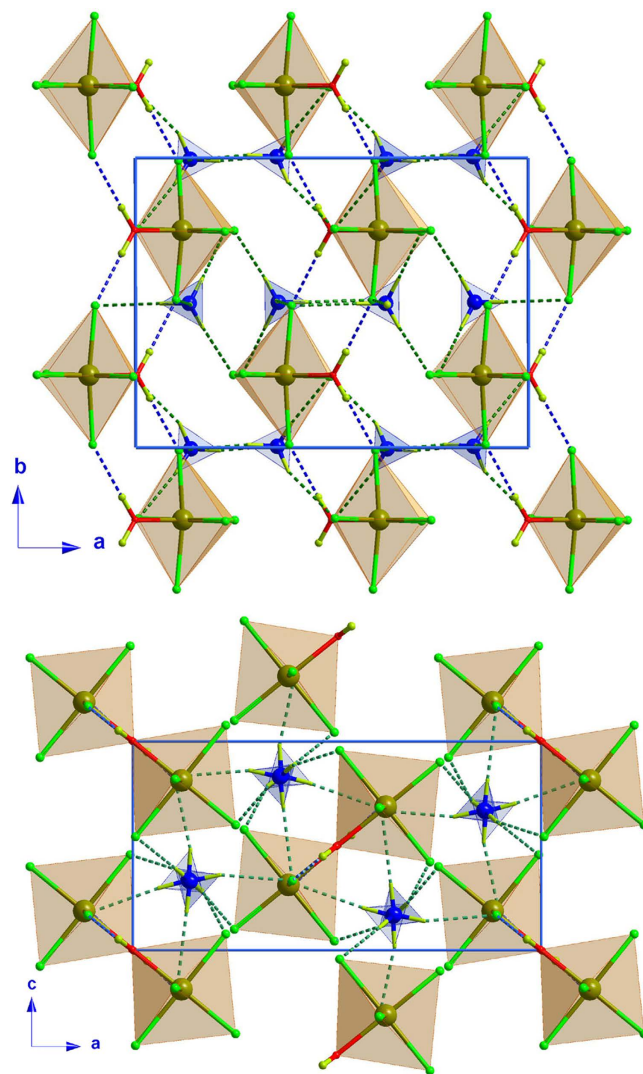
Figure 2. Views of the 2 K crystal packing along the *c*-axis (top) and *b*-axis (bottom) of (ND$_4$)$_2$[FeCl$_5$(D$_2$O)] compound, where the O-D···Cl and the N-D···Cl hydrogen bonds have been represented as blue and green dashed lines, respectively.

In order to fit successfully the experimental data, a combination of magnetic modes belonging to the Γ_1 and Γ_2 irreducible representations is required. The best solution was obtained with a cycloid model with moments mainly contained in the *ac*-plane and propagating along the *c*-direction (see Fig. 4). This corresponds to the admixture in phase quadrature of a mode along the *a*-axis belonging to Γ_1 and a mode along the *c*-axis belonging to Γ_2; it should be noted that the *v* and *q* component of the Γ_1 and Γ_2 irreducible representations permit a small component along the *b*-axis. This solution has been confirmed by global optimization using a simulated annealing procedure[28,29].

In the final refinements, the real and imaginary parts of the Fourier components S(j) were constrained to be equal, i.e. $m_{Fe} = |\text{Re}(Sj)| = |\text{Im}(Sj)|$, which corresponds to a spin cycloid with a circular envelope. The magnetic moments rotate within a plane that includes the propagation vector and which forms an angle of 4.4(1)° with the *ac*-plane. A refinement using an elliptical envelope instead (Re(Sj)≠Im(Sj)), does not improve significantly the agreement factors: the $R_F{}^2$ reaches a value of 12.6% and the difference between real and imaginary parts of the Fourier components is ca 0.3 μ_B. The best fit between the observed and calculated intensities was obtained with phase angles of zero for Fe(1) and Fe(3) and $\mathbf{k}_z/2$ for Fe(2) and Fe(4); therefore Fe(1) and Fe(3) as well as Fe(2) and Fe(4) are strictly antiparallel, while the angle between the magnetic moments of Fe(1)-Fe(4) and Fe(2)-Fe(3) is ca 41.5° (see Fig. 4). A full list of structural and magnetic parameters is given in Table 5, as well as the result of the magnetic refinement at 2 K (see also Supplementary Figure S3). The refined value of the Fe(III) magnetic moment, 3.805(2) μ_B, is in agreement with those previously reported for the family of general formula A$_2$[FeX$_5$(H$_2$O)], where A stands for an alkali metal or ammonium ion and X for a halide ion[26]. This value,

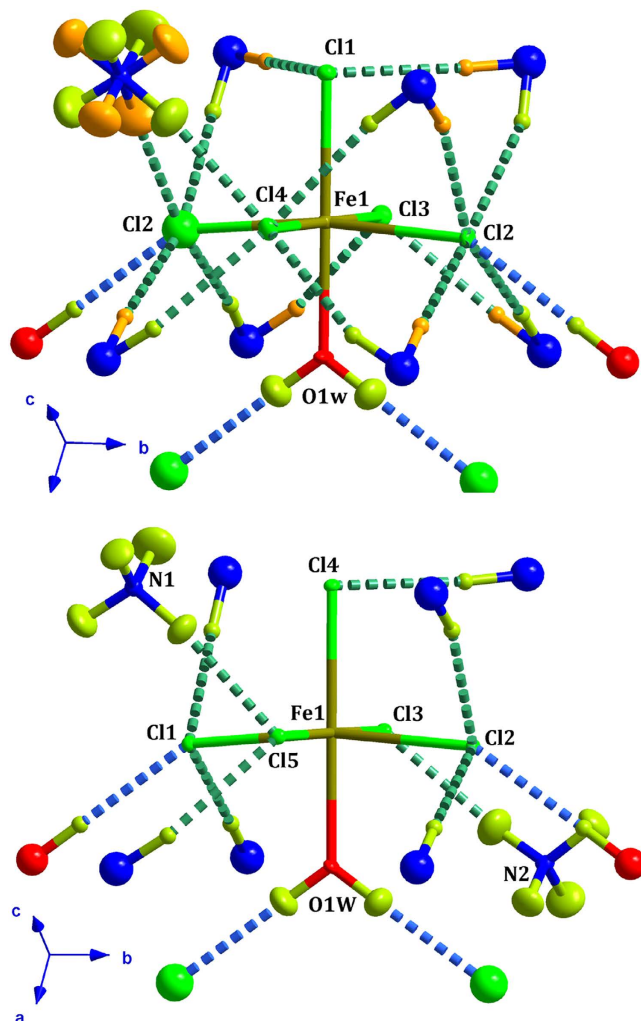**Figure 3. View of the hydrogen bond interactions between the [FeCl$_5$(D$_2$O)] unit and the adjacent molecules obtained from the neutron diffraction crystal structure at 100 (top) and 2 K (bottom).**
The O-D···Cl and the N-D···Cl hydrogen bonds have been represented as blue and green dashed lines, respectively. A detailed list of relevant hydrogen bond distances and angles can be consulted in Table 3. The asymmetric units are given in ORTEP representation with atoms at 50% of probability. Ammonium hydrogen atoms in the HT phase have been drawn on lime and orange colors in order to denote the two different conformations.

	Γ_1	Γ_2
$\mathbf{m}_{Fe(1)}$	(u, v, w)	(u, v, w)
$\mathbf{m}_{Fe(2)}$	$\varepsilon(-u, -v, w)$	$\varepsilon(u, v, -w)$
$\mathbf{m}_{Fe(3)}$	(p, q, r)	(p, q, r)
$\mathbf{m}_{Fe(4)}$	$-\varepsilon(-p,-q,r)$	$-\varepsilon(p, q,-r)$

Table 4. Magnetic moments of the content of a primitive cell deduced for the two possible irreducible representations (Γ_1 and Γ_2), for the magnetic sites: Fe(1)$_{4e}$ = (0.388, 0.249, 0.313), Fe(2)$_{4e}$ = (0.119, 0.751, 0.813), Fe(3)$_{4e}$ = (0.619, 0.751, 0.687) and Fe(4)$_{4e}$ = (0.881, 0.249, 0.187). The symmetry operators relating the positions are: (1) = x, y, z; (2) = $-x+1/2$, $-y+1$, $z-1/2$; $\varepsilon = \exp\{-i\cdot2\pi\cdot 0.1136\}$

slightly below the expected for a Fe(III) ion, indicates a non-negligible spin delocalization from the Fe(III) ions to the coordinated chloride atoms[35].

The admixture of two magnetic modes belonging to different irreducible representations lowers the point symmetry to m (*ab*-mirror plane) in perfect agreement with the emergence of an electrical polarization (**P**) in the *ab*-plane.
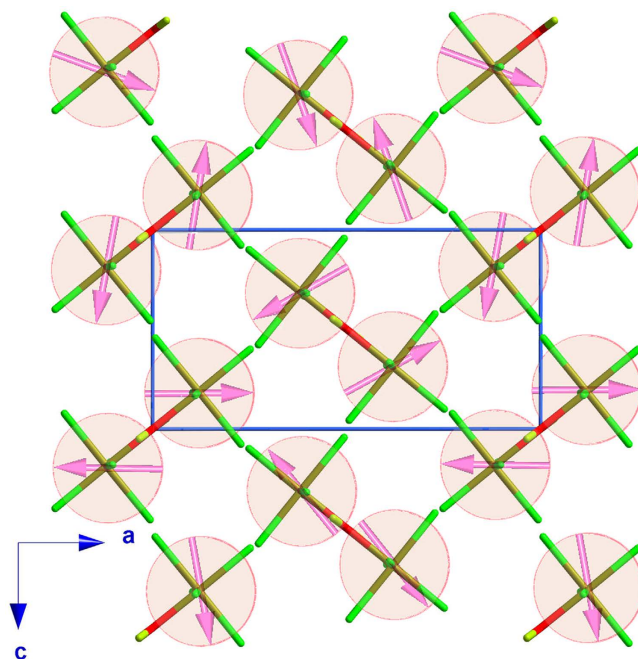
Figure 4. View along the *b*-axis of the superposition of the nuclear and magnetic structures for the combination of Γ_1 and Γ_2 irreducible representations. For the sake of clarity only [FeCl$_5$(D$_2$O)] units, have been represented. It should be noted that this combination of irreducible representations produces the same chirality for every spin chain running along the *c*-axis.

a(Å)	13.5019(7)	b(Å)	9.9578(5)	c (Å)	6.9049(4)
α (°)	90.00	β (°)	90.00	γ (°)	90.109(4)
k	(0,0,k_z)	k_z	0.2288(4)	M_{Fe} (μ_B)	3.805(2)
$\varphi(1)(2\pi)$	0.0	$\varphi(2)(2\pi)$	0.1136	Ext. Model[a]	Anisotropic
ϕ_{Re}(°)	177.11(6)	ϕ_{Im}(°)	−92.89(6)	R_{exp}(%)	4.25
θ_{Re}(°)	90.0	θ_{Im}(°)	175.6(1)	R_F(%)	12.8

Table 5. Magnetic parameters of (NH$_4$)$_2$[FeCl$_5$(H$_2$O)] obtained from the refinement of the magnetic reflections recorded at 2 K. ϕ and θ are the spherical angles of the Fourier components of the magnetic moment (real and imaginary). [a]Fixed values from the structural refinement at 2 K.

The presence of cycloids rotating in the *ac*-plane (with a small tilt of 4.4° along *b*) suggests that **P** should be preferentially directed along the *a*-axis, through the spin current mechanism induced via the inverse Dzyaloshinskii-Moriya interaction. The small tilt of the cycloid rotation plane towards *b*, is consistent with the weak electric polarization component along the *b*-axis previously observed[25].

The symmetry of the magnetic structure is consistent with either a first-order transition or two successive transitions, the latter being consistent with the presence of two anomalies observed in the low temperature region of the heat capacity (ca 6.9 and 7.2 K). This scenario is also in agreement with experiments conducted by Mössbauer spectroscopy[33,36,37] and muon spin relaxation[38], both pointing to the occurrence of two distinct magnetic structures. This sequence of transitions suggests that two order parameters directed respectively along the *a*− or *c*− crystallographic axis (and belonging to Γ_1 and Γ_2), condense in turn at T_{FE} and T_N. This corresponds to a transition on warming from cycloidal ($T < T_{FE}$) to collinear structure ($T_{FE} < T < T_N$), the latter involving a single irreducible representation and being compatible with the absence of electric polarization since this phase preserves inversion symmetry[25]. In fact, this would be reminiscent of the scenario observed in other compounds like TbMnO$_3$ or MnWO$_4$, where indeed such a sequence of two magnetic transitions is observed[3–9].

This hypothesis is reinforced by the temperature dependence of selected magnetic Bragg intensities such as (0, −3, k_z) and (0, 0, −1−k_z) recorded in the temperature range of 2–12 K (see Fig. 5). The first one shows a continuous decrease with increasing temperature up to its complete disappearance at T_N. In contrast, the second presents a discontinuous change in the slope at ca. 6.9 K, in correspondence with the lowest temperature peak observed in heat capacity and with the onset of electric polarization[25]. However, the variation in intensity of these magnetic reflections does not allow to determine unambiguously the
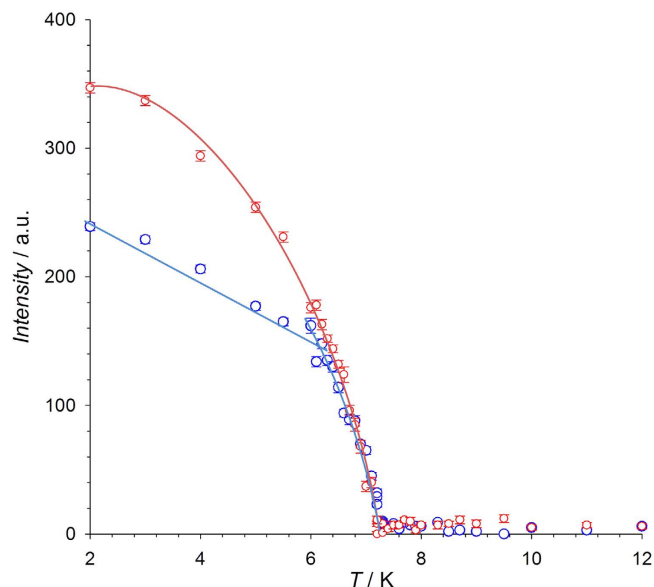
Figure 5. **Temperature evolution of the $(0, 0, -1-k_z)$ and $(0, -3, k_z)$ magnetic reflections, represented as blue and red circles, respectively.** The change of curvature in the $(0, 0, -1.23)$ reflection could be associated to a magnetic phase transition from cycloid to collinear magnetic structure. The solid lines are guides to the eye.

exact nature of the magnetic phase at $T_{FE} < T < T_N$. Moreover, the decrease of magnetic intensities in the vicinity of the paramagnetic region precludes the measurement of a full set of magnetic reflections.

The proposed magnetic structure at zero magnetic field can be explained by simple considerations regarding the exchange integrals, discussed using the notation already employed in ref 35. All magnetic exchange couplings are mediated by super-super exchange interactions, either through Cl-Cl or Cl-water pathways, and bound to be antiferromagnetic in nature. From previous DFT calculation in the $K_2[FeCl_5(H_2O)]$ compound[39], J_1, that couples Fe(1)-Fe(3) and Fe(2)-Fe(4) ions, must be the strongest interaction due to the short halogen-oxygen distance together with the enhancement of the magnetic interaction due to the well oriented hydrogen bond. Indeed our magnetic configuration shows that the spins of these pairs of ions are strictly antiparallel. For the sake of simplicity, we assume $J_1 = 1$ for the rest of the discussion.

The next most relevant topological feature is the presence of buckled anisotropic triangular layers lying in the bc-plane, involving the J_2 and J_4 interactions (see Fig. 6). This minimal set of parameters (J_1, J_2, J_4) allows to obtain a magnetic ground state which reproduces the experimental wave-vector $(k_z = 0.23)$, since for classical Heisenberg spins, the analytic solution of the anisotropic triangular lattice (J_2/J_4) is a spiral structure with $k_z = 2 \cdot a\cos[J_2/(2 \cdot J_4)]$. In the present case, one can derive $J_4 \approx 2/3 \cdot J_2$. It shall be noted that exact diagonalization of the first-ordered ground state shows that the minimum energy for any set $\{J_1, J_2, J_3, J_4\}$ is either at the Gamma point or along the Λ symmetry line $(0, 0, k_z)$ in CDML (Cracknell, A. P., Davies, B.L., Miller, S. C. and Love, W. F.) notation[40].

The magnetic structure determined experimentally shows that the relative angles between spins on neighboring sites are slightly different from those obtained using $\{J_1, J_2, J_4\}$ alone. A more realistic solution matching closely the observed angles requires the addition of a weak J_3 coupling. By including J_3 however, the J_4/J_2 ratio must be renormalized in order to preserve the experimental wave-vector. For example, for $J_3 = 0.1$, and $J_4/J_2 \approx 0.75$, the magnetic structure can be fully reproduced. A weaker J_3/J_4 ratio compared to that reported for the $K_2[FeCl_5(H_2O)]$ compound seems compatible with the shorter Cl(5)···O(1w) and Cl(3)···Cl(4) distances mediating the J_4 coupling. The set of exchange couplings proposed here may not be a unique solution since some values were arbitrarily fixed, but their relative magnitude $(J_1 > J_2 > J_4 > J_3)$ are consistent with the observed structure. *Ab-initio* calculations and/or measurements of magnetic excitations are required to provide quantitative values of these exchange couplings.

Discussion

With the ultimate goal of establishing the mechanism at the origin of multiferroicity in the title compound, we have carried out crystal and magnetic structure studies as a function of the temperature.

In previous works, the transition identified at 79 K by heat capacity measurements was hypothetically attributed to a structural phase transition, but all efforts to determine the crystal structure below this temperature led to solutions indistinguishable from the high temperature structure. In this work, we have taken advantage of the contrast provided by neutron diffraction for the precise determination of the positions of light atoms (in this case mainly the hydrogen/deuterium atoms of the ammonium
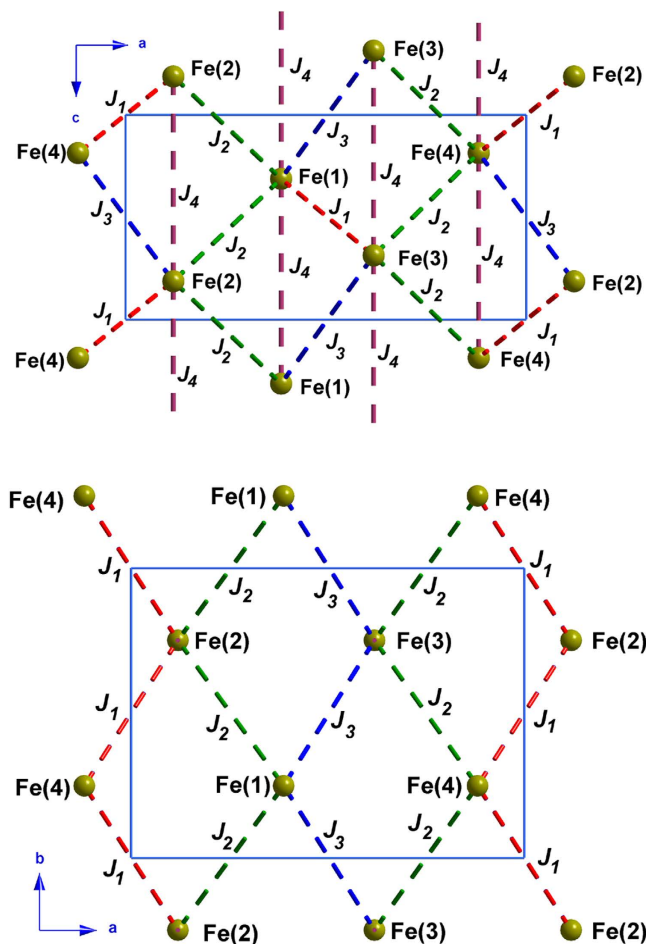
Figure 6. View along *b*- and *c*-axis of the four magnetic interactions using to model the magnetic ground state at 2 K (see main text). The different exchange couplings have been represented in color dashed lines. For the sake of clarity only the Fe(III) ions have represented.

molecules) to characterize this structural phase transition, which is ultimately explained by a blocking of the ammonium counterions.

The space group analysis at low temperature has shown that the title compound crystalizes in the $P112_1/a$ space group. The centrosymmetric character of the space group precludes ferroelectric polarization, as in fact is observed in the previously reported pyroelectric current measurements just below the structural phase transition[25].

The compound becomes magnetically ordered at 7.2 K (T_N) and becomes ferroelectric below 6.9 K (T_{FE}), with a spontaneous electric polarization presenting two different components: a strong one along the *a*-axis and a weak one along the *b*-axis, with a value ten times lower. Our magnetic neutron diffraction unambiguously shows that at 2 K, an incommensurate cycloidal spin structure is stabilized in zero magnetic field. The magnetic moments are contained mostly in the *ac*-plane (ca 4° tilt along *b*) and propagate along the *c*-direction. The symmetry lowering at 2 K confirms that the ferroelectricity is a direct consequence of the complex magnetic ordering and suggests that the *inverse* Dzyaloshinskii-Moriya mechanism is at play in the magnetoelectric coupling. This is in sharp contrast with all other compounds of the series (A$_2$[FeX$_5$(H$_2$O)] , where A stands for an alkali metal and X is an halogen atom) presenting commensurate collinear antiferromagnetic structures and not ferroelectric. This highlights that subtle chemical modifications produce remarkable changes in the physical behavior of this class of compounds. Specifically, the substitution of the alkali-metal for an ammonium molecule modifies the exchange coupling interactions giving rise to a frustrated magnetic structure. We have provided a minimalistic model based on a set of four isotropic exchange interactions which explains well the observed magnetic state. Strong competition within anisotropic triangular layers seems to be responsible for the observed behavior. It is likely that external parameters such as magnetic field or pressure influence drastically the spin state and potentially lift the frustration, as recently suggested from magnetoelectric measurements under external magnetic field. Further neutron diffraction experiments under external magnetic field are needed in order to elucidate the different magnetic models and determine the mechanism of magnetoelectric coupling in the different regions of the phase diagram.

Methods

Materials.   Deuterated reagents and solvents used in the synthesis were purchased from commercial sources and used without further purification. The synthesis of non-deuterated samples has been carried out with the same protocol described below but with hydrogenated reagents.

Synthesis of $(ND_4)_2[FeCl_5(D_2O)]$.   Single crystals of $(ND_4)_2[FeCl_5(D_2O)]$ of suitable size for neutron scattering were prepared by the seeded growth technique, by slow evaporation of saturated solutions at 50 °C. The seeds were formed by cooling of hot saturated solutions. The resulting compound was directly checked by single crystal X-ray diffraction and the results were in agreement with the unit cell parameters and the crystal structure previously reported[25,26].

X-ray Single Crystal Refinements.   Data collections of $(NH_4)_2[FeCl_5·H_2O]$ were carried out at room temperature (HT) and 50 K (LT) in an Agilent SuperNova X-ray μ-focus source equipped with a helium cryostream, using Mo-Kα radiation ($\lambda = 0.71073$ Å). The reflections were indexed, integrated and scaled using CrysAlis Pro program[41]. The structures of at HT and LT were solved by direct methods using the SHELXS97 program at the space group *Pnma* (No. 62). All non-hydrogen atoms were refined anisotropically by full-matrix least-squares technique based on F^2 using SHELXL97[32]. The hydrogen atoms were positioned geometrically and refined using the difference electron density map applying DFIX soft-constrains, giving rise to very close models for both temperatures; therefore no clear signal of the structural phase transition was observed. The only observed change comparing the HT with the LT measurements is the cell volume compression, which is around 2%, value which is compatible with the thermal expansion effect. The final geometrical calculations and the graphical manipulations were carried out with PARST97[42], PLATON[43] and DIAMOND[44] programs.

Neutron Diffraction Measurements.   Single-crystal neutron diffraction data were collected at the hot-neutrons four-circle diffractometer D9 at Institut Laue Langevin (ILL, Grenoble, France) with a wavelength of 0.8322(1) Å obtained with a copper (220) monochromator operating in transmission geometry. D9 diffractometer is equipped with a 2D detector of 6×6 cm (32×32 pixels) that allows a reciprocal space survey. The crystal was mounted onto specific aluminum sample holders that produce a low background and sealed into a closed-cycle cryostat.

In order to determine the crystal structure above and below the nuclear phase transition (79 K) data collections consisting in a combination of omega- and omega-2theta-scans of each individual reflection where carried out at 100 and 2 K, yielding 4900 and 2710 independent reflections respectively. The cell parameters where obtained at both temperatures and the crystal structure refined at 100 K and accurately determined below the phase transition. Due to the occurrence of a magnetic propagation vector different of $\mathbf{k} = (0, 0, 0)$, nuclear and magnetic reflections are not overlapped below the magnetic phase transition (T_N ca 7.25 K) and therefore both the magnetic and nuclear phases can be measured independently. The magnetic structure was determined at 2 K from 127 independent reflections. Additionally, the evolution of two different magnetic reflections [$(0, 0, -1-k_z)$ and $(0, -3, k_z)$] was followed in the temperature range from 2 to 12 K. The main experimental and crystallographic data are summarized in Table 1.

The program RACER[45] was used to integrate the omega- and omega-2theta-scans and to correct them for the Lorentz factor. The crystal attenuation corrections were performed with a prism model using DATAP program[46], with an estimated total neutron absorption coefficient of 0.057 cm^{-1} [47]. Additional high-resolution neutron powder diffraction measurements at D2B instrument (ILL) were performed at 45 K in order to verify the structural transformation at 79 K. The sample was contained in a Ø 6 mm cylindrical vanadium-can inside an Orange Cryostat. The neutron diffraction pattern was collected using 1.5642 Å wavelength.

The refinements of the nuclear structures were performed using the programs SHELX[32] and FullProf Suite[28,29]. The magnetic structure was treated with the program FullProf using the integrated intensities obtained from the single-crystal measurements. The models for the magnetic structure were deduced from the symmetry analysis techniques implemented in the program BasIreps included in the FullProf Suite[28,29]. The magnetic moments were localized on the Fe(III) atoms and, in the final refinement, the real and imaginary parts of the Fourier coefficients of the magnetic moments were constrained to have the same magnitude with directions described by spherical angles. The nuclear and magnetic contributions to the diffraction intensities were treated as two separate patterns, with the magnetic phase described in space group *P*-1 (No. 2), using the magnetic form-factor curve of Fe(III) and the scale factor obtained from the refinement of the nuclear phase at the same temperature.

References

1. Fiebig, M. Revival of the magnetoelectric effect *J. Phys. D* **38,** R123 (2005).
2. Toledano, P. Pseudo-proper ferroelectricity and magnetoelectric effects in TbMnO3. *Phys. Rev. B* **79,** 094416 (2009)
3. Goto, T., Kimura, T., Lawes, G., Ramirez, A. P. & Tokura, Y. Ferroelectricity and giant magnetocapacitance in perovskite rare-earth manganites *Phys. Rev. Lett.* **92,** 257201 (2004).
4. Van Aken, B. B., Palstra, T. T. M., Filippetti, A. & Spaldin, N. A. The origin of ferroelectricity in magnetoelectric YMnO3. *Nature Materials* **3,** 164 (2004).
5. Sergienko, I. A. & Dagotto, E. Role of the Dzyaloshinskii-Moriya interaction in multiferroic perovskites *Phys. Rev. B* **73,** 094434 (2006).

6. Kimura, T., Lawes, G., Goto, T., Tokura, Y. & Ramirez, A. P. Magnetoelectric phase diagrams of orthorhombic RMnO3 (R=Gd, Tb, and Dy) *Phys. Rev. B* **71,** 224425 (2005).
7. Taniguchi, K., Abe, N., Takenobu, T., Iwasa, Y. & Arima, T. Ferroelectric polarization flop in a frustrated magnet MnWO4 induced by a magnetic field *Phys. Rev. Lett.* **97,** 097203 (2006).
8. Arkenbout, A. H., Palstra, T. T. M., Siegrist, T. & Kimura, T. Ferroelectricity in the cycloidal spiral magnetic phase of MnWO4 *Phys. Rev. B* **74,** 184431 (2006).
9. Heyer, O. *et al.* A new multiferroic material: MnWO4 *J. Phys.: Condens. Matter* **18,** L471 (2006).
10. Yamasaki, Y. *et al.* Magnetic reversal of the ferroelectric polarization in a multiferroic spinel oxide *Phys. Rev. Lett.* **96,** 207204 (2006).
11. Tomiyasu, K., Fukunaga, J. & Suzuki, H. Magnetic short-range order and reentrant-spin-glass-like behavior in CoCr2O4 and MnCr2O4 by means of neutron scattering and magnetization measurements *Phys. Rev. B* **70,** 214434 (2004).
12. Dzyaloshinskii, I. A thermodynamic theory of "weak" ferromagnetism of antiferromagnetics. *J. Phys. Chem. Solids* **4,** 241 (1958).
13. Moriya, T. Anisotropic superexchange interaction and weak ferromagnetism *Phys. Rev.* **120,** 91 (1960).
14. Katsura, H., Nagaosa, N. & Balatsky, A. V. Spin current and magnetoelectric effect in noncollinear magnets *Phys. Rev. Lett.* **95,** 057205 (2005).
15. Harter, A., Cage, B., Nguyen, P., Abboud, K. A. & Dalal, N. S. (NH4)(3)CrO8: A new S=1/2 system exhibiting no magnetic transition down to 0.3 K *Polyhedron* **24,** 2350 (2005).
16. Cage, B. & Dalal, N. S. Unhydrated Cr(V) peroxychromates M3CrO8 (M = Na, K, Rb): Low-dimensional antiferromagnets exhibiting large specific heats at mK to 5 K temperatures. *Chem. Mater.* **13** 880 (2001).
17. Samantaray, R., Clark, R. J., Choi, E. S., Zhou, H. & Dalal, N. S. $M_{3-x}(NH_4)_{(x)}CrO_8$ (M = Na, K, Rb, Cs): A New Family of Cr^{5+}-Based Magnetic Ferroelectrics *J. Am. Chem. Soc.* **133,** 3792 (2011).
18. Samantaray, R., Clark, R. J., Choi, E. S. & Dalal, N. S. Elucidating the Mechanism of Multiferroicity in (NH4)(3)Cr(O-2)(4) and Its Tailoring by Alkali Metal Substitution. *J. Am. Chem. Soc.* **134** 15953 (2012).
19. Sánchez-Andújar, M. *et al.* First-order structural transition in the multiferroic perovskite-like formate [(CH3)(2)NH2][Mn(HCOO)(3)]. *CrystEngComm*, **16,** 3558 (2014).
20. Liu, B., Shang, R., Hu, K.-L., Wang, Z.-M. & Gao S. A New Series of Chiral Metal Formate Frameworks of [HONH3][M-II(HCOO) (3)] (M=Mn, Co, Ni, Zn, and Mg): Synthesis, Structures, and Properties *Inorg. Chem.* **51(24),** 13363 (2012).
21. Xu, G.-C., Ma, X.-M., Zhang, L., Wang, Z.-M. & Gao S. Disorder-Order Ferroelectric Transition in the Metal Formate Framework of [NH4][Zn(HCOO)(3)] *J. Am. Chem. Soc.* **132(28),** 9588 (2010).
22. Xu, G.-C. *et al.* Coexistence of Magnetic and Electric Orderings in the Metal-Formate Frameworks of [NH4][M(HCOO)(3)] *J. Am. Chem. Soc.* **133(38),** 14948 (2011).
23. Cañadillas-Delgado, L. *et al.* The Role of Order-Disorder Transitions in the Quest for Molecular Multiferroics: Structural and Magnetic Neutron Studies of a Mixed Valence Iron(II)-Iron(III) Formate Framework. *J. Am. Chem. Soc.* **134(48),** 19772 (2012).
24. Jain, P. *et al.* Multiferroic Behavior Associated with an Order-Disorder Hydrogen Bonding Transition in Metal-Organic Frameworks (MOFs) with the Perovskite ABX(3) Architecture. *J. Am. Chem. Soc.* **131(38),** 13625 (2009).
25. Ackermann, M., Brüning, D., Lorenz, T., Becker, P. & Bohatý L. Thermodynamic properties of the new multiferroic material (NH4)(2)[FeCl5(H2O)] *New Journal of Physics* **15,** 123001 (2013).
26. Carlin, R. L. & Palacio, F. The $A_2[FeX_5(H_2O)]$ series of antiferromagnets. *Coord. Chem. Rev.* **65,** 141 (1985).
27. Kitajgorodskii, A. I. *Molecular Crystals and Molecules*, New-York, Academic Press, (1973).
28. Rodríguez-Carvajal, J. Recent advances in magnetic structure determination by neutron powder diffraction. *Physica B* **192,** 55 (1993).
29. http://www.ill.eu/sites/fullprof/ Rodriguez-Carvajal, J., FullProf Suite Homepage, (2015) (Date of access: 21/04/2015).
30. Rubín, J., Palacios, E., Bartolomé, J. & Rodríguez-Carvajal J. A single-crystal neutron diffraction study of NH_4MnF_3. *J. Phys.: Condens. Matter* **7,** 563 (1995).
31. These values are within the range observed in the Cambridge Structural Database (CSD) http://www.ccdc.cam.ac.uk/pages/Home.aspx (Date of access: 01/10/2014).
32. Sheldrick, G. M. A short history of SHELX. *Acta Cryst.* **A64,** 112 (2008).
33. Partiti, C. S. M., Rechenberg, H. R. & Sanchez, J. P. The influence of NH4+ ionic motion on the magnetic structure of $(NH_4)_2FeCl_5.H_2O$: a Mossbauer study. *J. Phys. C: Solid State Phys.* **21,** 5825 (1988).
34. Bertaut, E. F. in: Magnetism, Eds. Rado, G. T. & Shul H. Academic: NewYork Vol.III, *Chap.4* (1963).
35. Luzón, J., Campo, J., Palacio, F., McIntyre, G. J. & Millán, A. Understanding magnetic interactions in the series $A_2FeX_5 \cdot H_2O$ (A=K, Rb, X=Cl, Br). I. Spin densities by polarized neutron diffraction and DFT calculations *Phys. Rev. B* **78,** 054414 (2008).
36. Calage, Y., Dormann, J. L., Moron, M. C. & Palacio, F. Mössbauer study of $(NH_4)_2FeCl_5.H_2O$. *Hyp. Interact.* **54,** 483 (1990).
37. Brown, S. R. & Hall, I. A Mössbauer study of $(NH_4)_2FeCl_5.H_2O$. *J. Phys.: Cond. Matter* **4,** 9191 (1992).
38. Attendoborough, M., Hall, I., Nikolov, O. & Brown, S. R. A muon spin relaxation study of the magnetic ordering of $(NH_4)_2FeCl_5.H_2O$ *Hyp. Interact.* **108,** 435 (1997).
39. Campo, J. *et al.* Understanding magnetic interactions in the series $A_2FeX_5 \cdot H_2O$ (A=K, Rb, X=Cl, Br). II. Inelastic neutron scattering and DFT studies. *Phys. Rev. B* **78,** 054415 (2008).
40. Cracknell, A. P., Davies, B. L., Miller, S. C. & Love, W. F. Kronecker Product Tables. Vol. 1. *General Introduction and Tables of Irreducible Representations of Space Groups.* New York: IFI/Plenum (1979).
41. Agilent. CrysAlis PRO Agilent Technologies Ltd, Yarnton, England, (2010).
42. Nardelli, M. PARST95—an update to PARST: a system of Fortran routines for calculating molecular structure parameters from the results of crystal structure analyses. *J. Appl. Crystallogr.* **28,** 659 (1995).
43. Spek, A. L. Single-crystal structure validation with the program PLATON *J. Appl. Cryst.* **36,** 7 (2003).
44. DIAMOND 2.1d, Crystal Impact GbR, CRYSTAL IMPACT, K. Brandenburg & H. Putz GbR, Postfach 1251, D-53002 Bonn, Germany, (2000).
45. Lehmann, M. S. & Larsen, F. K. A method for location of the peaks in step-scan measured Bragg reflexions Lehmann. *Acta Cryst.* **A30,** 580 (1974).
46. Coppens, P. Crystallographic Computing, Ed. F. R. Ahmed Munksgaard International Booksellers and Publishers Ltd. Copenhagen 255 (1979).
47. Howard, J. A. K., Johnson, O., Schultz, A. J. & Stringer, A. M. Determination of the neutron absorption cross section for hydrogen as a function of wavelength with a pulsed neutron source Howard *J. Appl. Cryst.* **20,** 120 (1987).

Acknowledgements

Author Contributions

L.C., J.C., O.F. and J.A.R.V. conceived the project. O.F., A.M. and J.A.R.V. prepared the samples. R.J. performed the x-ray diffraction measurements. O.F., L.C. and J.A.R.V. performed the neutron diffraction measurements and analysis and wrote the paper. All the authors commented and revised the paper.

Additional Information

Supplementary information accompanies this paper at http://www.nature.com/srep

Competing financial interests: The authors declare no competing financial interests.

How to cite this article: Alberto Rodríguez-Velamazán, J. *et al.* Magnetically-induced ferroelectricity in the $(ND_4)_2[FeCl_5(D_2O)]$ molecular compound. *Sci. Rep.* **5**, 14475; doi: 10.1038/srep14475 (2015).